The Astrophysical Journal, 757:2 (16pp), 2012 September 20 doi:10.1088/0004-637X/757/1/2

GALAXIES IN X-RAY GROUPS. II. A WEAK LENSING STUDY OF HALO CENTERING

Matthew R. George[1,2], Alexie Leauthaud[3], Kevin Bundy[3], Alexis Finoguenov[4,5], Chung-Pei Ma[1], Eli S. Rykoff[2,6], Jeremy L. Tinker[7], Risa H. Wechsler[6,8], Richard Massey[9], and Simona Mei[10,11]
[1] Department of Astronomy, University of California, Berkeley, CA 94720, USA; mgeorge@astro.berkeley.edu
[2] Lawrence Berkeley National Laboratory, 1 Cyclotron Road, Berkeley, CA 94720, USA
[3] Kavli Institute for the Physics and Mathematics of the Universe (Kavli IPMU, WPI), Todai Institutes for Advanced Study, University of Tokyo, Kashiwa 277-8583, Japan
[4] Max-Planck-Institut für Extraterrestrische Physik, Giessenbachstraße, D-85748 Garching, Germany
[5] Center for Space Science Technology, University of Maryland Baltimore County, 1000 Hilltop Circle, Baltimore, MD 21250, USA
[6] Kavli Institute for Particle Astrophysics and Cosmology, SLAC National Accelerator Laboratory, 2575 Sand Hill Road, Menlo Park, CA 94025, USA
[7] Center for Cosmology and Particle Physics, Department of Physics, New York University, 4 Washington Place, New York, NY 10003, USA
[8] Physics Department, Stanford University, Stanford, CA 94305, USA
[9] Department of Physics, University of Durham, South Road, Durham DH1 3LE, UK
[10] Bureau des Galaxies, Etoiles, Physique, Instrumentation (GEPI), University of Paris Denis Diderot, F-75205 Paris Cedex 13, France
[11] GEPI, Observatoire de Paris, Section de Meudon, F-92195 Meudon Cedex, France
Received 2012 May 18; accepted 2012 July 19; published 2012 August 28

ABSTRACT

Locating the centers of dark matter halos is critical for understanding the mass profiles of halos, as well as the formation and evolution of the massive galaxies that they host. The task is observationally challenging because we cannot observe halos directly, and tracers such as bright galaxies or X-ray emission from hot plasma are imperfect. In this paper, we quantify the consequences of miscentering on the weak lensing signal from a sample of 129 X-ray-selected galaxy groups in the COSMOS field with redshifts $0 < z < 1$ and halo masses in the range 10^{13}–$10^{14}\ M_{\odot}$. By measuring the stacked lensing signal around eight different candidate centers (such as the brightest member galaxy, the mean position of all member galaxies, or the X-ray centroid), we determine which candidates best trace the center of mass in halos. In this sample of groups, we find that massive galaxies near the X-ray centroids trace the center of mass to $\lesssim$75 kpc, while the X-ray position and centroids based on the mean position of member galaxies have larger offsets primarily due to the statistical uncertainties in their positions (typically ∼50–150 kpc). Approximately 30% of groups in our sample have ambiguous centers with multiple bright or massive galaxies, and some of these groups show disturbed mass profiles that are not well fit by standard models, suggesting that they are merging systems. We find that halo mass estimates from stacked weak lensing can be biased low by 5%–30% if inaccurate centers are used and the issue of miscentering is not addressed.

Key words: cosmology: observations – galaxies: clusters: general – galaxies: groups: general – gravitational lensing: weak

Online-only material: color figures

1. INTRODUCTION

Galaxy groups and clusters are important sites of galaxy evolution, and the abundance of these massive objects provides a sensitive probe of the amplitude of matter fluctuations and other cosmological parameters. Analyses of these structures require some knowledge of the location of the centers of their gravitational potentials. Because the total mass distribution is dominated by dark matter and is not directly observable, halo centers are typically assumed to be traced by a massive galaxy or the density peak of radiating hot gas. Miscentering is a critical issue when estimating the masses of groups and clusters, because it adds significant systematic uncertainties (e.g., Johnston et al. 2007a, 2007b; Mandelbaum et al. 2010; Rozo et al. 2011) and also degrades constraints on the concentration of mass profiles (Mandelbaum et al. 2008). Velocity offsets between observational tracers and halo centers impact studies of satellite kinematics (Skibba et al. 2011; Wojtak et al. 2011) and redshift-space distortions (Hikage et al. 2012). On the other hand, offsets between observational tracers and the true halo centers can provide information about the dynamical state of these systems and about the properties of dark matter (Clowe et al. 2006; Massey et al. 2011).

Finding halo centers is challenging for a number of reasons. Galaxy formation models (as well as halo models for describing the multiplicity of galaxies within halos) typically place the brightest or most massive galaxy at the center of each halo. But the brightest galaxy in a cluster is not always the central galaxy (Skibba et al. 2011, and references therein). Groups and clusters form from mergers of halos where the most massive halo becomes the host halo with its central galaxy, and smaller halos become subhalos with satellite galaxies. Several analyses of data from group catalogs and field surveys have found that there is some intrinsic scatter in stellar mass and luminosity at fixed halo mass (Yang et al. 2009; More et al. 2009; Leauthaud et al. 2012; Reddick et al. 2012), which implies that halos can end up with satellites that are intrinsically more massive or luminous than the central galaxy. Additionally, there are uncertainties in measuring any observable quantity such as stellar mass that can cause a satellite to be misidentified as the most massive central galaxy, and structure projected along the line of sight can confuse the identification of member galaxies. Another difficulty is that merging systems are dynamically unrelaxed, which can produce offsets between the central galaxy and the halo center or other tracers such as the X-ray center. The systematics introduced by picking centers that do not coincide with the "true" center of mass are important and need to be quantified.

Gravitational lensing is a powerful tool for finding the centers of mass of halos since it is sensitive to the total mass distribution along a line of sight. Mass maps can be

constructed for individual systems with strong lensing or for massive clusters with weak lensing (e.g., Smith et al. 2005; Oguri et al. 2010; Shan et al. 2010). Such studies often find reasonable agreement between the positions of bright massive galaxies, X-ray emission, and lensing mass peaks, with a handful of interesting examples that illustrate how dark matter peaks can be offset from hot gas in merging galaxy clusters (e.g., Clowe et al. 2004; Bradač et al. 2008).

In this paper, however, we are concerned with a large statistical sample of groups with lower masses and higher redshifts, a regime of interest for many current and future weak lensing surveys. The typical signal-to-noise ratio for the weak lensing signal from individual groups is low, so we cannot identify their halo centers individually. By stacking the lensing signal from many groups, we determine the mean mass profile around a given center. We repeat this process for different candidate centers and compare the resulting profiles to find the best tracer of the center of mass. The center of a smooth halo can be identified as the position where the lensing signal is maximized on small scales. Other components such as a massive galaxy or subhalo that is offset from the halo center could produce an additional peak in the lensing signal, so we must account for that when modeling the signal.

We analyze a sample of 129 X-ray-selected galaxy groups at redshifts $0 < z < 1$ from the COSMOS field (Scoville et al. 2007), described in George et al. (2011). With COSMOS data, we have X-ray luminosities and centroids for each group, with member galaxies identified using photometric redshifts derived from over 30 ultraviolet, optical, and infrared bands, and a subsample with spectroscopic redshifts. We use weak lensing measurements from high-resolution *Hubble* imaging to study the accuracy with which tracers such as bright galaxies and X-ray emission identify the centers of dark matter halos.

This paper is the second in a series studying the galaxy content of X-ray groups. George et al. (2011, hereafter Paper I) presented a catalog of group membership assignments from a Bayesian treatment of photometric redshifts, along with extensive tests of the selection algorithm using mock catalogs and subsamples with spectroscopic redshifts. Initial analyses of group members were used in that paper to demonstrate an environmental influence on galaxy colors out to $z = 1$. A previous weak lensing study of this group sample was used to constrain the mean relation between X-ray luminosity and halo mass (Leauthaud et al. 2010).

In this paper we study the centers of groups in detail to optimize observational choices for centering, to study the impact of miscentering on measurements of halo properties, and to explore the effects of merging and substructure on lensing measurements. The outline of the paper is as follows. Section 2 describes the data used in our analysis, including the X-ray group catalog, assignment of member galaxies, and lensing shape measurements. We define eight candidate group centers in Section 3 and describe our procedure for testing different choices of centers in Section 4. Section 5 presents the results of our analysis, and Sections 6 and 7 provide discussion and conclusions of our work.

We adopt a WMAP5 ΛCDM cosmology with $\Omega_m = 0.258$, $\Omega_\Lambda = 0.742$, $H_0 = 72\ h_{72}$ km s^{-1} Mpc^{-1} (Dunkley et al. 2009) following the initial lensing analysis of these groups by Leauthaud et al. (2010). All distances are expressed in physical units with $h = 0.72$. X-ray luminosities are expressed in the 0.1–2.4 keV band, rest frame. All magnitudes are given on the AB system. To approximate the virial radii of halos, we use R_{200c}, which is the radius within which the mean mass density equals 200 times the critical density of the universe at the halo redshift, $\rho_c(z)$. The corresponding mass enclosed within this radius is $M_{200c} = 200\rho_c(4\pi/3)R^3_{200c}$. We also assume that halos follow a Navarro–Frenk–White (NFW, Navarro et al. 1996) density profile, with a concentration parameter c_{200c} and a scale radius $R_s = R_{200c}/c_{200c}$. We use the term "group" to denote a set of galaxies occupying a common halo, and the halo masses of these groups are in the range 10^{13}–$10^{14}\ M_\odot$ as estimated with weak lensing (Leauthaud et al. 2010). We will generally refer to more massive structures as clusters following convention, but we make no other physical distinction between groups and clusters.

2. DATA

To study how the constituents of galaxy groups trace the centers of mass of dark matter halos, we use an X-ray-selected sample of galaxy groups from the COSMOS field (Scoville et al. 2007). We refer the reader to Paper I for details of the data and methods used to construct the group catalog, as well as tests of its properties with simulations and spectroscopic data. In this section, we briefly describe aspects of the catalog that are relevant for centering, including the assignment of member galaxies to groups. We also introduce the galaxy shear catalog used in our weak lensing analysis.

2.1. X-Ray Group Catalog

Our sample of galaxy groups has been selected from an X-ray mosaic combining images from the *XMM-Newton* (Hasinger et al. 2007) and *Chandra* (Elvis et al. 2009) observatories following the procedure of Finoguenov et al. (2009, 2010). A wavelet filtering of the X-ray mosaic is used to distinguish extended structures on scales of 32″ and 64″ from contaminants on smaller scales like active galactic nuclei. Once extended X-ray sources are detected, a red sequence finder is employed on galaxies with a projected distance less than 0.5 Mpc from the centers to identify an optical counterpart and determine the redshift of the group, which is then refined with spectroscopic redshifts when available.

A quality flag (hereafter XFLAG) has been assigned to each group based on the reliability of the optical counterpart identification. We study groups with XFLAG = 1 or 2, indicating a confident spectroscopic association, while higher values indicate uncertain counterparts that could be due to projection effects or photometry contaminated by bright foreground stars. Sources with XFLAG = 1 also have clear X-ray centroids, with an uncertainty in each position coordinate, σ_X, equal to the wavelet scale of 32″ divided by the signal-to-noise ratio of the flux measurement, while sources with XFLAG = 2 have less certain X-ray centroids, for which we have $\sigma_X = 32''$ set by the wavelet scale of the flux measurement.

To ensure a clean sample of groups with robust membership assignment, we employ the additional quality cuts suggested in Paper I, excluding groups that are near field edges or have significantly masked areas, potentially merging groups identified as distinct X-ray sources but with significantly overlapping volumes, and poor groups with fewer than four members identified. After these quality cuts, we have 129 groups in our sample ranging from redshift $0 < z < 1$.

2.2. Galaxy Membership

To determine how well galaxies trace the matter distribution in groups, we must first identify the galaxies that reside in

them. The COSMOS field has extensive imaging in over 30 ultraviolet, optical, and infrared bands (Capak et al. 2007), enabling the determination of stellar masses (see Paper I for details) and precise photometric redshifts (Ilbert et al. 2009, and Paper I for further tests). In Paper I, we presented a catalog of member galaxies for these X-ray groups, selected according to their photometric redshifts and proximity to X-ray centroids. Briefly, a Bayesian membership probability, $P_{\rm mem}$, is assigned to each galaxy by comparing the photometric redshift probability distribution function to the expected redshift distribution of group and field galaxies near each group. From the list of members with $P_{\rm mem} = 1 - P_{\rm field} > 0.5$, the galaxy with the highest stellar mass within an NFW scale radius of the X-ray centroid (including the positional uncertainty, $\sigma_{\rm X}$) is selected as the group center. We call this object the $\rm MMGG_{scale}$ for "most massive group galaxy within a scale radius." A final membership probability is assigned by repeating the selection process within a new cylinder recentered on this galaxy.

We have extensively tested this selection algorithm using mock catalogs and with subsamples of galaxies for which we have spectroscopic redshifts and found it to be both pure and complete near group centers; within $0.5R_{200c}$ and down to our limiting selection magnitude (F814W = 24.2), 84% of galaxies selected as group members truly belong in groups, and 92% of true group members are selected as such. In this paper we use the member catalog derived from photometric redshifts, which has an average of 26 members per group. From that list, there are an average of 6 members per group with spectroscopic redshifts for calibration and determining group redshifts.

2.3. Weak Lensing Data

The galaxy shape measurements used for our weak lensing analysis are described in Leauthaud et al. (2007). These are derived from high-resolution imaging over 1.64 deg^2 of the COSMOS field with the Advanced Camera for Surveys (ACS) on the *Hubble Space Telescope* (*HST*; Koekemoer et al. 2007) to a limiting magnitude of F814W = 26.4. Variations in the point-spread function (PSF) with position and time are modeled following Rhodes et al. (2007), and galaxy shapes are derived using the RRG method (Rhodes et al. 2000). The PSF-corrected shapes are converted to estimators of shear, γ, using a shear susceptibility factor calculated from moments of the global distribution of shapes and a calibration factor determined from simulated images. Updates to the procedure and the shear catalog are described in detail elsewhere in Leauthaud et al. (2012). These improvements include a more detailed correction of charge transfer inefficiency from Massey et al. (2010) and an empirical derivation of the dispersion in shear measurements in bins of magnitude and detection significance. This estimate of the shear dispersion includes contributions from intrinsic shape noise and shape measurement uncertainties and varies from $\sigma_\gamma \approx 0.25$ for bright galaxies to $\sigma_\gamma \approx 0.40$ for faint objects.

The stacked weak lensing signal is derived from the average tangential shear, $\gamma_t(R)$, of background source galaxies at a projected distance R from the center of each group. The shear is related to the excess surface mass density $\Delta\Sigma(R)$ (Miralda-Escude 1991)

$$\Delta\Sigma(R) \equiv \overline{\Sigma}(< R) - \overline{\Sigma}(R) = \gamma_t(R)\Sigma_{\rm crit}, \quad (1)$$

where $\overline{\Sigma}(< R)$ is the mean surface density within radius R and $\overline{\Sigma}(R)$ is the azimuthally averaged surface density at R. The critical surface density $\Sigma_{\rm crit}$ is a function of the angular diameter distances between the observer (O), lens (L), and source (S),

$$\Sigma_{\rm crit} = \frac{c^2}{4\pi G}\frac{D_{OS}}{D_{OL}D_{LS}}, \quad (2)$$

where c is the speed of light and G is the gravitational constant.

In order to compute $\Sigma_{\rm crit}$ from Equation (2), we need to know the distances to both the sources and lenses. The group catalog provides lens redshifts that come primarily from spectroscopic data including zCOSMOS (Lilly et al. 2009; S. J. Lilly et al. 2012, in preparation). For background sources, we use photometric redshifts from Ilbert et al. (2009). To avoid contamination due to uncertainties in photometric redshifts, we use only sources with $z_S - z_L > \max[0.1, \sigma_z]$, where σ_z is the 68% uncertainty in the source redshift. We also exclude sources with a secondary peak in their redshift density function (i.e., $\rm zP_2 \neq 0$ in the Ilbert et al. 2009 catalog) that have a significant fraction of catastrophic redshift errors. With these cuts, the source catalog contains 210,015 galaxies with well-measured shapes and redshifts, providing a source density of 36 galaxies arcmin^{-2}.

To obtain a significant measurement of $\Delta\Sigma$, we must combine the signal from many lenses and background sources. The combined measurement is a weighted sum over pairs of lenses i and sources j,

$$\Delta\Sigma = \frac{\sum_i \sum_j \mathcal{W}_{ij}\gamma_{t,ij}\Sigma_{{\rm crit},ij}}{\sum_i \sum_j \mathcal{W}_{ij}}, \quad (3)$$

where the weight $\mathcal{W}_{ij} = (\Sigma_{\rm crit}\sigma_{\gamma,ij})^{-2}$ is the inverse variance of the measurement. We measure $\Delta\Sigma$ in annular bins from 20 kpc to 1 Mpc. Covariance between measurements becomes an issue on larger scales, where background sources can be paired with multiple lenses, but this is not significant over the scales we measure. Uncertainties in $\Delta\Sigma$ are determined from the inverse square root of the sum of the weights of lens–source pairs.

3. DEFINING CANDIDATE CENTERS

The "center" of a galaxy group requires some definition. There is ambiguity in centering even when considering simulated dark matter halos; the mass centroid, most bound particle, and density peak can all be different because of asphericity and substructure. The choice of group and cluster centers in observational data sets is further limited by the available measurements. Here, we review a variety of definitions of group centers and their relative advantages. Our aim is to use weak lensing to determine which candidates most accurately trace (on average) the centers of mass of dark matter halos. We will consider a variety of candidate centers and begin by studying the level of agreement between them. Our choice of candidate centers is meant to explore the range of options available for multi-wavelength data sets while using a simple set of rules for identification; however, it is not an exhaustive list of possible centers.

It is useful to separate these definitions into two broad categories. We call the first set "galaxy candidates," since they are centered on a single galaxy, and the second set "centroid candidates," which are defined for a spatially extended quantity like the galaxy density field or X-ray emission and are in general not centered on an individual galaxy. Some centering algorithms take a hybrid approach, using the proximity of neighboring members to ultimately select a luminous galaxy (e.g., Robotham et al. 2011), but we do not test those methods here.

When identifying centers based on the galaxy content of groups, we select from galaxies with membership probability $P_{\rm mem} > 0.5$, as described in Section 2.2 and Paper I. Though the list of members is defined around one of the candidate centers (the $\rm MMGG_{scale}$), the radius ($R_{\rm 200c}$) used to select members is large enough that the initial choice of center should not impact our results. Each of the centers based on galaxy fluxes (e.g., brightest group galaxy) uses the observed magnitude in the F814W band, taken with the ACS on *HST*, with no corrections for dust or evolution. Since these measurements do not account for the change in rest-frame wavelength probed, they will be more sensitive to recent star formation at higher redshifts. Centers based on galaxy masses use the full measured spectral energy distribution (SED), so these effects are diminished.

3.1. Galaxy Candidate Centers

Many clusters have a central dominant galaxy with an extended stellar envelope, often located near the density peak of hot intracluster gas as seen in X-rays and the peak of the matter density probed by lensing or kinematics (e.g., Lin & Mohr 2004, and references therein). This motivates the choice of a single galaxy to trace the centers of groups and clusters. The general picture is further supported by numerical simulations of dark matter halos and subhalos and has been encapsulated in the halo model, which successfully describes many aspects of large-scale structure, including measurements of galaxy clustering and lensing (e.g., Cooray & Sheth 2002; Zehavi et al. 2005; Mandelbaum et al. 2006b; Leauthaud et al. 2012).

Thus, a popular choice when defining cluster centers in optical catalogs is the brightest cluster galaxy (BCG; or BGG in groups), since the selection is relatively simple (e.g., Koester et al. 2007b; Hao et al. 2010). But the choice of filter and aperture used for the flux measurement has an impact on which galaxies are selected; differences in redshift, star formation history, and dust content affect the flux observed in a given band, so a single flux measurement cannot reflect the complicated physical processes occurring in group centers. Color cuts can be used to isolate a few of these effects (e.g., Gladders & Yee 2000), though they often come with assumptions about the properties of central galaxies. For example, some group catalogs use the brightest red sequence galaxy to identify group centers, avoiding galaxies that are bright due to recent star formation in favor of massive galaxies with old stellar populations.

Stellar masses are a promising alternative to observed or rest-frame luminosities since they correlate more directly with the masses of halos in which galaxies reside. However, stellar mass estimates require more detailed measurements of the SEDs of galaxies and are fraught with larger uncertainties than simple fluxes or luminosities.

In this paper we consider four galaxy candidates, selected based on flux or stellar mass and distance to the X-ray position:

1. $\rm MMGG_{scale}$: the galaxy within $R_s + \sigma_{\rm X}$ of the X-ray centroid having the greatest stellar mass.
2. $\rm MMGG_{R200}$: the galaxy having the greatest stellar mass of all group members within $R_{\rm 200c}$.
3. $\rm BGG_{scale}$: the brightest galaxy within $R_s + \sigma_{\rm X}$ of the X-ray centroid.
4. $\rm BGG_{R200}$: the brightest galaxy of all group members within $R_{\rm 200c}$.

The X-ray centroid (with uncertainty $\sigma_{\rm X}$) is used as the starting point for selecting these galaxies because it should roughly trace the halo center and we do not have lensing centers for individual groups. Note that there is not necessarily a galaxy within the NFW scale radius R_s of the X-ray centroid, so $\rm MMGG_{scale}$ and $\rm BGG_{scale}$ are not necessarily defined for all galaxy groups. However, in the case of our clean sample, each group has at least one member within this radius, so we do not have to deal with undefined centers. Uncertainties in the galaxy positions are much smaller than the sizes of the galaxies and are therefore negligible compared to the offsets from halo centers that we are capable of measuring with weak lensing.

3.2. Centroid Candidate Centers

The central galaxy is not always observationally obvious, and selection of an incorrect galaxy can produce statistically undesirable results when studying a sample of groups or clusters. This problem has motivated the use of centroids based on the positions of some or all group members, which can be weighted by their properties such as flux or stellar mass, with the hope that a robust statistic can be less prone to large errors than the choice of a single galaxy (e.g., White et al. 1999; Carlberg et al. 2001; Berlind et al. 2006; Jee et al. 2011).

Additionally, other probes of groups and clusters such as X-ray and SZ (Sunyaev & Zeldovich 1972) observations of hot gas and gravitational lensing can be used to find halo centers. Deep pointed observations can map the gas distribution in great detail for bright systems that are nearby or massive, but centering uncertainties can be significant for fainter systems (see Section 2.1). Similarly, only very massive systems produce a large enough lensing signal to study their spatial mass distribution individually, and lower mass systems (like the groups studied here) require stacking, such that centroids cannot be determined for each individual group from lensing alone.

Here we consider four centroid candidates:

1. CN: the centroid of member galaxies.
2. CM: the centroid of member galaxies weighted by stellar mass.
3. CF: the centroid of member galaxies weighted by flux.
4. X-ray: the X-ray centroid.

Uncertainties on the X-ray positions were discussed in Section 2.1 and have a mean value of 22″ or 134 kpc. For the other centroid candidates (CN, CM, and CF), the coordinates are computed using a weighted mean,

$$\mathbf{x}_{\rm cen} = \frac{\sum_{i=1}^{N} w_i \mathbf{x_i}}{\sum_{i=1}^{N} w_i}, \quad (4)$$

where $\mathbf{x_i}$ is the pair of coordinates (R.A., Decl.)$_i$ for each galaxy i, N is the number of group members, and w_i is the appropriate galaxy weight for each center definition; $w_i = 1, M_{\star,i}, f_i$ for CN, CM, CF, respectively, where $M_{\star,i}$ is the stellar mass and $f_i \propto 10^{-0.4 m_i}$, with f_i and m_i the flux and apparent F814W magnitude for each galaxy, respectively. We estimate the errors for these weighted means using bootstrap resampling from the list of member galaxies. With an average of 26 member galaxies per group, the mean statistical uncertainties on the projected galaxy centroid positions are 45, 52, and 50 kpc for candidates CN, CM, and CF, respectively, where we have taken the geometric mean of the uncertainties in two dimensions and converted the angular uncertainty to a projected physical distance at the redshift of each group. Groups with a higher projected density of member galaxies tend to have smaller centroid uncertainties, but improvements appear to be limited by contamination in the outskirts from correlated structure

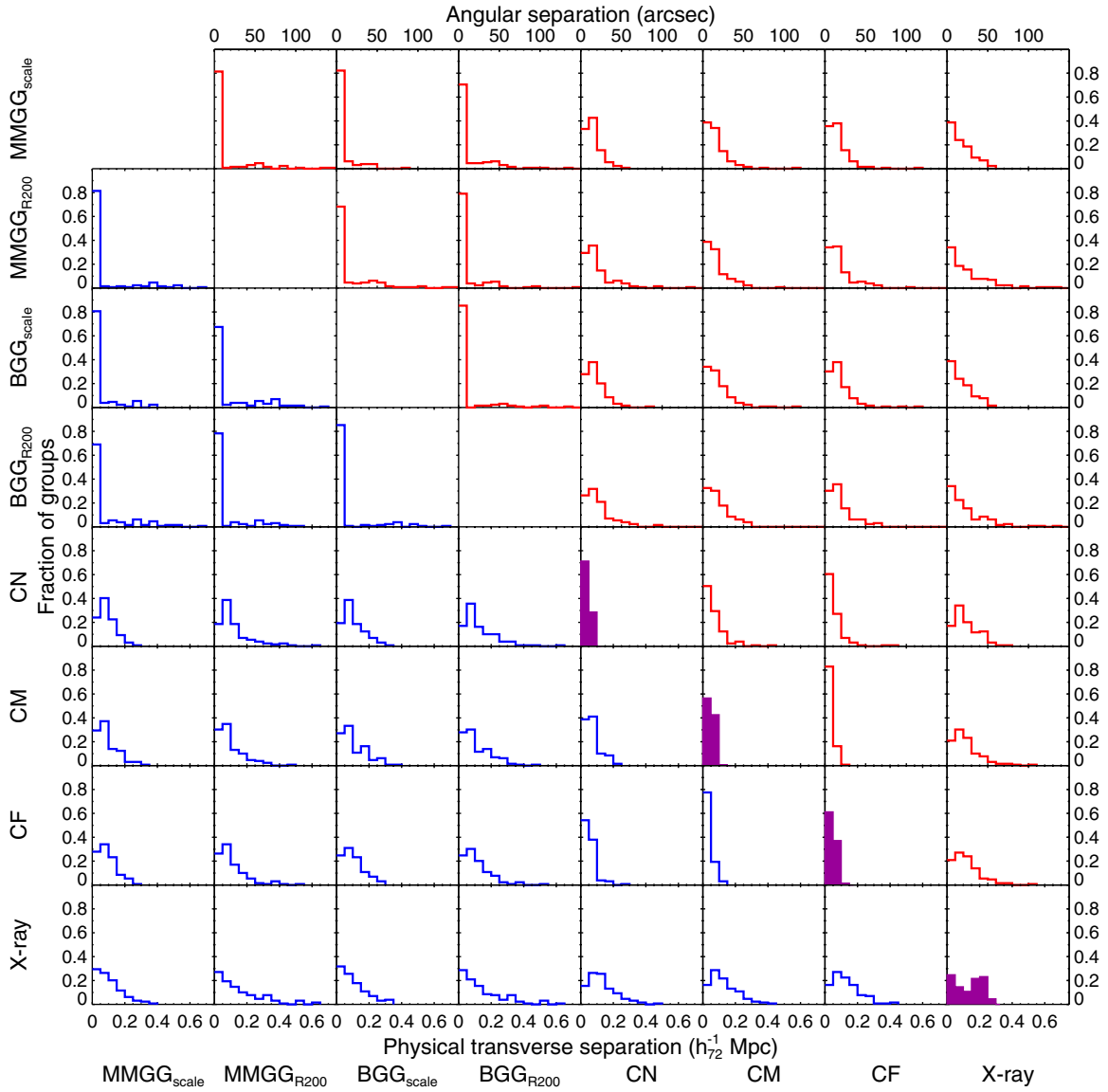

Figure 1. Distribution of projected offsets between pairs of candidate centers in our group sample, measured in arcseconds (upper right; red) and Mpc (lower left; blue). The angular and physical offset distributions are not identical because the groups span a range of redshifts. The filled purple histograms on the diagonal panels show the distribution of statistical uncertainties for each centroid position, described in Section 2.1 for the X-ray centroid and Section 3.1 for the others. The *y*-axis gives the fraction of groups in each bin; bin sizes are 50 Mpc (bottom left and diagonal) and 10″ (upper right).

(A color version of this figure is available in the online journal.)

(see Paper I for tests of purity and completeness). We have tested different centroiding schemes, including iterating until the centroid and member list converge or restricting to red galaxies, but achieved qualitatively similar results as with the centroids presented.

3.3. Offsets Between Candidate Centers

Our first test of these various centers is to see how well they agree with one another. Figure 1 shows the distribution over all groups of the angular and physical distance offsets between pairs of candidate centers, along with the distribution of uncertainties in centroid positions. Immediately, we see that candidate centers do not always agree. For example, in 22% of groups the brightest galaxy within R_{200c} is not the most massive galaxy and the candidates are separated by up to several hundred kpc. The agreement level among pairs of galaxy candidates is typically 70%–80% with a long tail in the distribution extending out roughly to the virial radius for these groups. The galaxy candidates are typically offset from the centroid candidates by 50–100 kpc, again with tails of a few hundred kpc, and the centroid candidates are in slightly better agreement among themselves. The offsets between the X-ray centroid and other candidate centers are generally consistent with the statistical uncertainties on the X-ray centroid. When comparing galaxy centroids (CN, CM, and CF) to other candidate centers, the typical offsets are roughly consistent with the mean uncertainty on the centroid position, but there are long tails in the offset distribution that exceed typical uncertainties.

These results are generally consistent with offsets found in other groups and cluster samples, though direct comparison is difficult given the variety of methods and data used for identifying objects and their centers. For ∼30% of optically selected groups in a similar mass range as our sample, Skibba et al. (2011) found that the brightest galaxy was not the central one, based on the relative positions and velocities

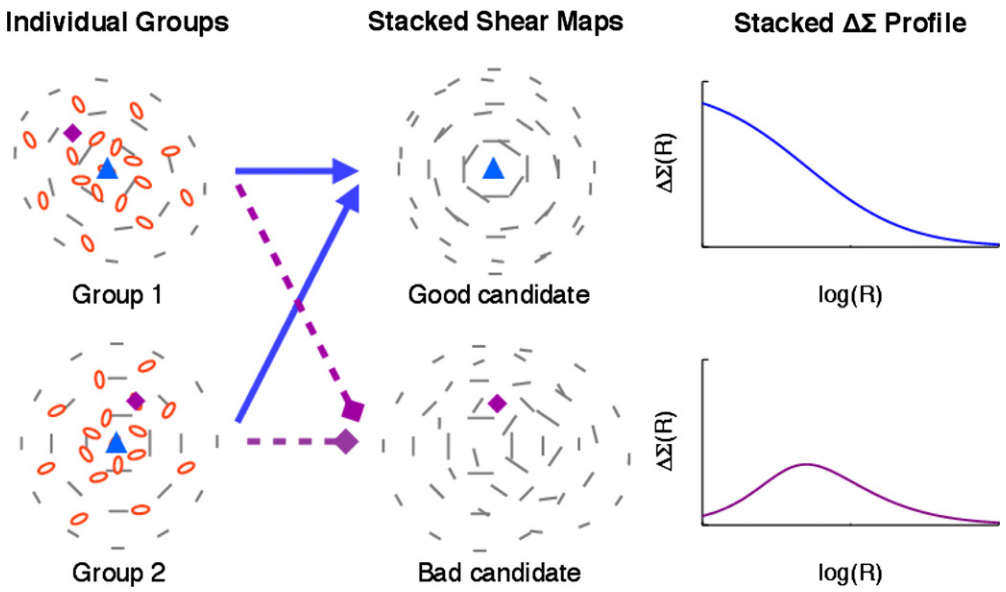

Figure 2. Schematic illustration of stacked lensing around different candidate centers. Candidate centers are defined in each group (left), and then shear maps are stacked around each position (middle) and azimuthally averaged to compute $\Delta\Sigma$ profiles (right).

(A color version of this figure is available in the online journal.)

of other member galaxies. This is comparable to the level of disagreement we find between our galaxy candidates, for which choosing a central galaxy is ambiguous. Comparing the positions of BCGs to X-ray centroids in 42 optically selected clusters, Sheldon et al. (2001) noted a mean offset of 85 kpc. With an expanded sample of 94 clusters with matching X-ray detections, Koester et al. (2007a) found a very similar median BCG-X-ray offset of 81 kpc and noted ∼20% of systems with offsets of several hundred kpc, which were mostly due to confusion in identifying the X-ray position or BCG. In a study of 65 massive clusters with higher quality X-ray data, Sanderson et al. (2009) found BCG-X-ray offsets of typically less than a few tens of kpc, with a few outliers that were merging systems. Our X-ray offsets are somewhat larger due to the statistical uncertainties in the centroid positions, with a mean (median) offset of 104 kpc (78 kpc) between the $\mathrm{MMGG_{scale}}$ and X-ray centroid.

4. WEAK LENSING METHODOLOGY

4.1. The Approach

Our stacked weak lensing approach to test candidate centers is sketched in Figure 2. The left column shows two separate galaxy groups (red ellipses) and their corresponding shear maps measured from the shapes of background galaxies (gray sticks). For each group, two candidate centers are defined (blue triangle and purple diamond), and the shear maps are stacked around these positions in the middle column. The rightmost panels show the resulting lensing signal $\Delta\Sigma$ as measured radially from the candidate center. We emphasize that the lensing signal for individual groups studied in this paper is noisy (signal-to-noise ratio ∼1; see Figure 1 of Leauthaud et al. 2010), so we cannot directly identify the centers of weak lensing maps for individual groups and must stack many groups; in this sense Figure 2 is exaggerated.

Qualitatively, the amplitude of the lensing signal is maximized when the lens position used for stacking coincides with the true center of mass in each system, and the signal is suppressed when the nominal position deviates from the true center of mass. The two curves agree at radii much larger than the typical centering offset. More formally, the lensing signal around miscentered halos was first studied in the context of satellite galaxies (Natarajan & Kneib 1997; Hudson et al. 1998; Guzik & Seljak 2002; Yang et al. 2003, 2006) and later applied to the problem of uncertain group centers (Johnston et al. 2007a, 2007b).

Observationally, our aim is to find the candidate center that maximizes the lensing signal on small scales, indicating that it best traces the center of mass. Furthermore, we would like to model the signal to infer the underlying mass profile and the typical offsets between our tracers and the true center of mass in halos. Interpreting the signal is complicated by a number of effects, including the shapes of halo profiles and the properties of galaxies and subhalos, which will be discussed further in Section 6.

4.2. Models

To interpret the mean lensing signal $\Delta\Sigma$ defined in Equations (1) and (3), we construct a model for the surface mass density $\Sigma(R)$ of a typical lens. Contributions to $\Sigma(R)$ in our group sample come primarily from the dark matter halo and the central galaxy (if the center is defined to be at the position of a galaxy). The parameters of the model are introduced in Table 1. We include three variants of the model: a *centered* version where the halo center is fixed at the position of the candidate center, an *offset* model that allows a distribution of offsets between the candidate and true halo center, and the *full* model, which adds freedom to the halo profile and allows for excess mass in the form of a subhalo around the candidate center.

We model the average mass density in halos with a spherical NFW profile, for which the projected surface density $\Sigma_{\rm halo}(R) = \Sigma_{\rm NFW}(R)$ is given in, e.g., Wright & Brainerd (2000), with halo mass and concentration as two free parameters. For the centered and offset models we will assume a mass–concentration relation from Zhao et al. (2009), leaving mass as a single free parameter for the halo component, while both mass and concentration are free parameters in the full model.

Table 1
Model Parameters for $\Delta\Sigma(R)$

Parameter	Description	Centered	Offset	Full	Prior Mean	Prior σ	Restrictions
$\log(M_{200c}/M_\odot)$	Halo mass	Free	Free	Free	13.5	0.8	...
c_{200c}	Halo concentration	Tied	Tied	Free	4.0	3.0	$1 < c_{200c} < 10$
σ_{off}(kpc)	Offset distance scale	Fixed	Free	Free	0	200	$\sigma_{off} > 0$
$\log(M_{gal}/M_\odot)$	Stellar mass	Fixed	Fixed	Fixed	$\langle\log(M_{\star,gal}/M_\odot)\rangle$	...	...
$\log(M_{sub}/M_\odot)$	Subhalo mass	Omitted	Omitted	Free	$\langle\log(M_{\star,gal}/M_\odot)\rangle$	1.0	$\log(M_{sub}/M_\odot) > 10$

Notes. For each model, $M_{\star,gal}$ is fixed to the mean photometrically estimated stellar mass of the central galaxy (for galaxy candidates) and zero otherwise. For the centered and offset models, halo concentration is set by the relation of Zhao et al. (2009).

When the surface density of a spherically symmetric halo is measured around the correct center of mass, we have $\overline{\Sigma}(R) = \Sigma_{halo}(R)$. If there is an offset R_{off} in the lens plane between the true center and the position used for measurement, the surface density measured at the coordinates (R, θ) relative to the offset position is (Yang et al. 2003, Appendix B)

$$\Sigma^{off}_{halo}(R, \theta | R_{off}) = \Sigma_{halo}\left(\sqrt{R^2 + R^2_{off} - 2RR_{off}\cos\theta}\right). \quad (5)$$

The azimuthally averaged surface density around the offset position is

$$\overline{\Sigma}^{off}_{halo}(R|R_{off}) = \frac{1}{2\pi}\int_0^{2\pi} d\theta\, \Sigma^{off}_{halo}(R, \theta|R_{off}). \quad (6)$$

For an ensemble of halos with a distribution of offsets $P(R_{off})$, Johnston et al. (2007a, 2007b) generalized Equation (6) to give the mean azimuthally averaged surface mass profile stacked around the offset positions

$$\overline{\Sigma}^{off}_{halo}(R|P(R_{off})) = \int_0^\infty P(R_{off})\,\overline{\Sigma}^{off}_{halo}(R|R_{off})\, dR_{off}. \quad (7)$$

The mean surface density inside a radius R is

$$\begin{aligned}\overline{\Sigma}^{off}_{halo}(<R|P(R_{off})) &= \frac{1}{\pi R^2}\int_0^R\int_0^{2\pi}\int_0^\infty P(R_{off})\,\Sigma^{off}_{halo}(R', \theta|R_{off}) \\ &\quad \times R' dR' d\theta dR_{off} \\ &= \frac{2}{R^2}\int_0^R \overline{\Sigma}^{off}_{halo}(R'|P(R_{off}))\, R' dR'. \end{aligned} \quad (8)$$

To model the lensing signal from a large sample of galaxy clusters centered around BCGs, Johnston et al. (2007b) used a distribution of offsets $P(R_{off})$ estimated from mock catalogs. In their model a fraction of BCGs correctly identified the centers of halos ($R_{off} = 0$), while the remaining clusters had a distribution of offsets given by

$$P(R_{off}) = \frac{R_{off}}{\sigma_{off}}\exp\left(-\frac{R^2_{off}}{2\sigma^2_{off}}\right). \quad (9)$$

This model, called a two-dimensional Gaussian or a Rayleigh distribution, was chosen based on mock catalogs to which their cluster-finding algorithm had been applied. The mocks suggested that the fraction of correctly centered clusters depended on richness, with higher richness clusters more likely to be centered correctly. In other clusters, the central galaxy was not correctly identified as the BCG, and the distribution of offsets between the BCG and true halo center could be described by Equation (9) with the parameter $\sigma_{off} = 420\,h^{-1}$ kpc describing the typical offset scale, independent of cluster richness.

We can think of the offset more generally in three dimensions, where we assume that the offset in each dimension is normally distributed with mean zero. The observed offset in the line-of-sight dimension might not have the same variance as the dimensions in the lens plane because of redshift-space distortions, but as long as the distribution in three dimensions is joint-normal and the variance in the two dimensions of the lens plane is equal, the projected offset distribution will take the form of Equation (9) after marginalizing over the line of sight.

The miscentering component employed by Johnston et al. (2007b) added two free parameters to their model: the fraction of miscentered groups and the scale length of the offset distribution. These additional parameters could not be well constrained by the data and had to be constrained using strong priors from mock catalogs.

Our approach is to use an offset model with a single free parameter to constrain the scale of the miscentering distribution empirically. We do not include separate components for centered and miscentered groups as Johnston et al. (2007b) did, as the single parameter model generally provides sufficient fits to the current data. Also, correctly chosen central galaxies may still be offset from their halo centers, an effect that was not included in the mocks of Johnston et al. (2007b) but has been tentatively seen in lensing maps of individual clusters (Oguri et al. 2010).

The second component of the model is the surface density contributed by the central galaxy, $\Sigma_{gal}(R)$. The shape of this mass profile is uncertain, but its contribution is subdominant even at the smallest radii that we probe ($R \sim 50$ kpc). For the centered and offset models, we simply model the galaxy component as a point source, $\Sigma_{gal}(R) = M_{gal}/(\pi R^2)$, with M_{gal} fixed to the average stellar mass $M_{\star,gal}$ of the central galaxies in the ensemble as estimated from their SEDs. The centroid candidates (CN, CM, CF, and X-ray) typically do not have a galaxy very near the center, so we do not include a contribution from Σ_{gal} when modeling the signal from these candidates.

We can write the centered and offset models as the sum of the halo and galaxy components:

$$\Delta\Sigma^{cen}(R) = \Delta\Sigma_{NFW}(R) + \Delta\Sigma_{gal}(R) \quad (10)$$

$$\Delta\Sigma^{off}(R) = \Delta\Sigma^{off}_{NFW}(R|P(R_{off})) + \Delta\Sigma_{gal}(R). \quad (11)$$

Note that $\Delta\Sigma^{cen}(R) = \Delta\Sigma^{off}(R|R_{off} = 0)$. We later test a scenario with the full model in which the candidate center has an additional mass component in the form of a dark matter subhalo that is more extended than the stellar profile, which will be described further in Section 5.3.

Though the measured signal is an ensemble average coming from halos with a range of masses and mass profiles, our

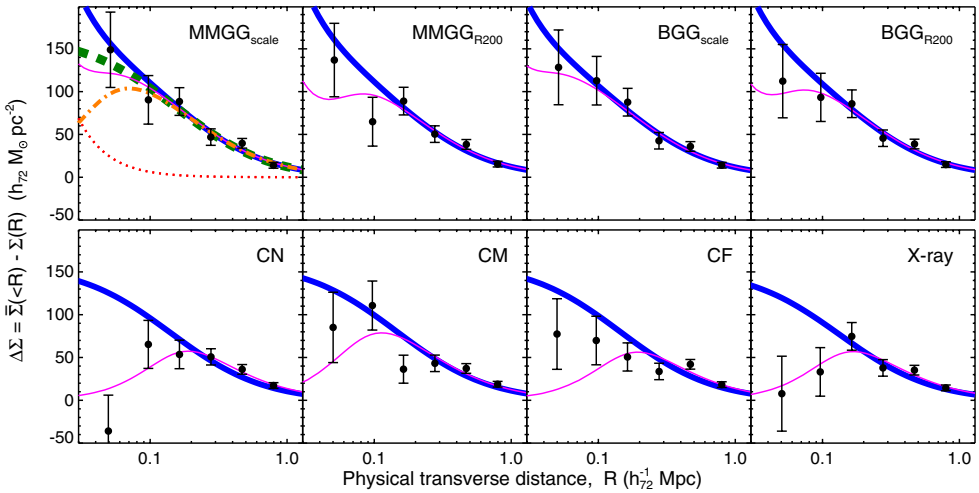

Figure 3. Weak lensing signal stacked on the full sample of groups around different centers, along with centered (thick blue; $\Delta\Sigma^{cen}$) and offset (thin magenta; $\Delta\Sigma^{off}$) models. Halo and central components of these models are shown for MMGG$_{scale}$ (green dashed for $\Delta\Sigma^{cen}_{NFW}$, orange dot-dashed for $\Delta\Sigma^{off}_{NFW}$, red dotted for $\Delta\Sigma_{gal}$). The top row shows the signal around galaxy candidates, while the bottom row shows centroid candidates. The signal (black points) is measured in radial bins, with the first spanning 20–70 kpc for sufficient signal-to-noise ratio and then logarithmically spaced from 70 kpc to 1 Mpc.

(A color version of this figure is available in the online journal.)

model consists of a single profile for simplicity and because the range of halo masses inferred from group X-ray luminosities is relatively small. We restrict our analysis of the lensing signal to $R < 1$ Mpc, where the effects of halo truncation and correlated structure should be unimportant to the lensing signal, and note that this adequately covers the range of centering offsets shown in Figure 1. At small scales, the assumption of weak shear becomes less accurate. Mandelbaum et al. (2006a) derive a correction term to the surface density contrast that depends on Σ_{crit} and $\Sigma(R)$ for the sample. These correction factors have been computed for this sample by Leauthaud et al. (2010) and shown to be fairly small on the scales we probe (of order 10% of the measured signal in our innermost bin for a good center), so we do not include them in our analysis.

To fit the models to the data, we attempt to find the parameters that minimize

$$\chi^2 = \sum_i \frac{(\Delta\Sigma_{data}(R_i) - \Delta\Sigma_{model}(R_i))^2}{\sigma_i^2}, \qquad (12)$$

where σ_i is the measurement uncertainty on $\Delta\Sigma_{data}(R_i)$. In practice, we use a Markov Chain Monte Carlo (MCMC) approach to efficiently explore the multi-dimensional parameter space maximizing the logarithm of the likelihood, $L \propto \exp(-\chi^2/2)$. We employ Gaussian or lognormal priors for each parameter, with means and standard deviations given in Table 1. The data are unable to constrain a lower limit to the subhalo mass or an upper limit to the concentration, so we restrict these parameters to $\log(M_{sub}/M_\odot) > 10$ and $c_{200c} < 10$ when they are free. We also require $c_{200c} > 1$ and $\sigma_{off} > 0$.

5. RESULTS

5.1. Weak Lensing on the Full Sample

Given that Figure 1 shows a wide range of offsets between different choices of group centers, we proceed to test how well the candidate centers trace the underlying matter distribution. We begin by studying the full sample of groups in this section, and in the next section we focus on the subset of groups with significant offsets between candidates.

For each center candidate, we measure the lensing signal $\Delta\Sigma(R)$ from all groups in annular bins around the center. The results are shown for the eight candidate centers in Figure 3. Each panel represents a different candidate center from Section 3, for which we plot the measured $\Delta\Sigma(R)$ (black points) along with models $\Delta\Sigma^{cen}(R)$ (thick blue) and $\Delta\Sigma^{off}(R)$ (thin magenta). For illustration, we show the halo and galaxy components of the models for MMGG$_{scale}$: $\Delta\Sigma_{NFW}(R)$ (green dashed), $\Delta\Sigma^{off}_{NFW}(R|R_{off})$ (orange dot-dashed), and $\Delta\Sigma_{gal}(R)$ (red dotted).

The mean and standard deviation (1σ) of the posterior distribution for each parameter, along with the mean central galaxy masses and χ^2 values for the fits, are shown in Table 2. The χ^2 values have not been normalized by the number of degrees of freedom ν. Each model is fit to six data points with one and two free parameters for the centered and offset models, respectively, so $\nu = 5$ for the centered model and $\nu = 4$ for the offset model. When $\chi^2 \approx \nu$, the model is consistent with the data given the uncertainties. A high value of χ^2 indicates that the model does not fit the data; for example, the data are inconsistent with the model at a 95% confidence level when $\chi^2 \geqslant 11.07(9.49)$ for $\nu = 5(4)$.

There are clear differences among the lensing signals for the eight candidate centers. The signal generally rises toward small scales for the galaxy candidates, while there is a turnover for the centroid candidates, indicating that they are poorer at tracing the center of mass in these groups. The stellar mass in the candidate central galaxies produces some of the difference in the signal, but the best-fit models show that the galaxy candidates have smaller offsets from the halo centers when compared with the centroid candidates even when accounting for the stellar mass. We will explore the possibility of additional mass in the central galaxy candidates in Section 5.3. It is important to note that the offsets measured from the lensing signals for the X-ray position and other centroid candidates are primarily due to the large statistical uncertainties in the centroid positions, shown in Figure 1. Figure 3 shows the impact of these centroid uncertainties on the lensing signal, but we cannot infer from these data that there are significant intrinsic offsets between the true centroid positions and the center of the dark matter halo.

For each of the galaxy candidates, the χ^2 value in Table 2 indicates that the centered model provides a good description

Table 2
Parameters Constraints for $\Delta\Sigma(R)$

Candidate	$\langle\log(M_{\star,\rm gal}/M_\odot)\rangle$	Centered Model			Offset Model			
		$\log(M_{200c}/M_\odot)$	c_{200c}	χ^2 ($\nu=5$)	$\log(M_{200c}/M_\odot)$	c_{200c}	$\sigma_{\rm off}$ (kpc)	χ^2 ($\nu=4$)
Galaxy candidates								
$\rm MMGG_{scale}$	11.3	13.43 ± 0.07	4.0	4.2	13.45 ± 0.07	3.9	18.2 ± 11.3	4.2
$\rm MMGG_{R200}$	11.4	13.43 ± 0.06	4.0	5.3	13.47 ± 0.07	3.9	28.3 ± 15.2	4.4
$\rm BGG_{scale}$	11.2	13.40 ± 0.06	4.0	2.9	13.43 ± 0.07	4.0	16.8 ± 10.0	2.8
$\rm BGG_{R200}$	11.3	13.42 ± 0.07	4.0	4.4	13.45 ± 0.06	3.9	24.8 ± 12.0	3.0
Centroid candidates								
CN	...	13.35 ± 0.07	4.0	21.0	13.51 ± 0.07	3.9	65.0 ± 18.0	2.8
CM	...	13.39 ± 0.07	4.0	10.5	13.45 ± 0.08	3.9	34.5 ± 21.6	9.3
CF	...	13.38 ± 0.07	4.0	14.0	13.51 ± 0.09	3.9	66.9 ± 29.9	9.5
X-ray	...	13.30 ± 0.08	4.1	15.2	13.42 ± 0.08	4.0	57.1 ± 16.9	3.5

Note. For both models, $M_{\star,\rm gal}$ is fixed to the stellar mass of the central galaxy (for galaxy candidates) and zero otherwise, and the halo concentration is fixed by the relation of Zhao et al. (2009).

of the data given the error bars. The extra degree of freedom in the offset model does not significantly improve the fit, and the constraints on $\sigma_{\rm off}$ are consistent with zero at the 2σ level. The best-fit values for $\sigma_{\rm off}$ and the quality of the fits are statistically consistent for each of the galaxy candidates, so we do not strongly favor one candidate over another, though there is marginal evidence that the candidates defined within an NFW scale radius of the X-ray position ($\rm MMGG_{scale}$ and $\rm BGG_{scale}$) trace the halo center slightly better than candidates defined over the larger area within R_{200c}.

On the other hand, the centered model generally does not provide good fits to the data for the centroid candidates, and the offset models do improve the fits. The best-fit offset parameter $\sigma_{\rm off}$ is significantly larger for the centroid candidates than for the galaxy candidates and deviates from zero by more than 2σ for three of the centroid candidates. The offset model fits two centroid candidates (CM and CF) only marginally well, so these would perhaps be better fit by a more complicated offset distribution.

The effect of miscentering on the halo mass constraints is comparable to the statistical uncertainty for this sample. The best-fit halo masses assuming a centered model for the centroid candidates tend to be $\sim 1\sigma$ lower than for galaxy candidates. Halo masses increase slightly when offsets are allowed in the model, and candidates with larger offsets are more affected. When miscentering is not accounted for in the model, halo masses are underestimated by 5%–30% compared to when we include the effect, depending on the choice of center.

We have also tested the effect of fixing the concentration parameter with our assumed mass–concentration relation, and freeing this parameter does not qualitatively change the results. We do not obtain a good constraint on the concentration, but the best-fit value for the galaxy candidates is consistent with our assumed value. The centroid candidates prefer somewhat lower concentrations, but the values are still consistent within the large error bars.

5.2. Groups with Discrepant Candidate Centers

While the stacked lensing signal for the full sample of groups shown in Figure 3 exposes differences between candidate centers, Figure 1 shows that the candidate centers are identical in many groups. In order to more directly compare different centering schemes, we now select only the groups in which candidate centers disagree by a measurable amount. Figures 4 and 5 present this analysis, with each row showing the lensing signal centered on the $\rm MMGG_{scale}$ (left column) and a different candidate (middle column) for the subset of groups where the two candidate centers are separated by more than 50 kpc. The rightmost column shows the histogram of offsets between the two centers repeating Figure 1 on logarithmic axes. The number of groups and the mean redshift of each subset are shown at the top right. We have chosen the $\rm MMGG_{scale}$ as a fiducial center here since Table 2 suggests that it is among the best candidates, but using the $\rm BGG_{scale}$ gives a consistent picture.

In each row of the figure, we first model the lensing signal in the left-hand panel assuming that the $\rm MMGG_{scale}$ correctly traces the halo center, fitting for the halo mass with concentration fixed. Next, we take that best-fit-centered model and convolve it with the distribution of offsets in the right-hand panel to model the signal in the middle panel. This is equivalent to replacing the offset distribution of Equation (9) with the empirical distribution of offsets between two candidates, leaving no free parameters for the models shown in the middle panels. We again add a central point mass fixed to the mean photometric stellar mass of the candidate galaxies for each of the galaxy centers. Though we expect that galaxies offset from the halo center have subhalos, the lensing data are currently insufficient to constrain such an additional contribution. The halo mass is fitted using only the lensing data centered on the $\rm MMGG_{scale}$, so the level of agreement between the offset model and the data in the middle panel can be read as a consistency test.

Looking first at the comparisons between the $\rm MMGG_{scale}$ and the centroid candidates in Figure 4, we see that the lensing signal is reasonably well described with an NFW halo centered on the $\rm MMGG_{scale}$, with a mean halo mass consistent with that measured for the full sample in Table 2. Additionally, the offset model gives a decent representation of the lensing signal measured around the centroid candidates shown in the middle panels. We interpret these results as indicating that centroid candidates do not trace halo centers as well as galaxy candidates.

In the samples where the $\rm MMGG_{scale}$ disagrees with other galaxy candidates (Figure 5), the lensing signal is different than in the centroid comparison. The best-fit halo masses are significantly lower than in the full sample measured earlier. The lensing signals are noisier, in part because of the smaller sample sizes, and one case deviates significantly from the offset

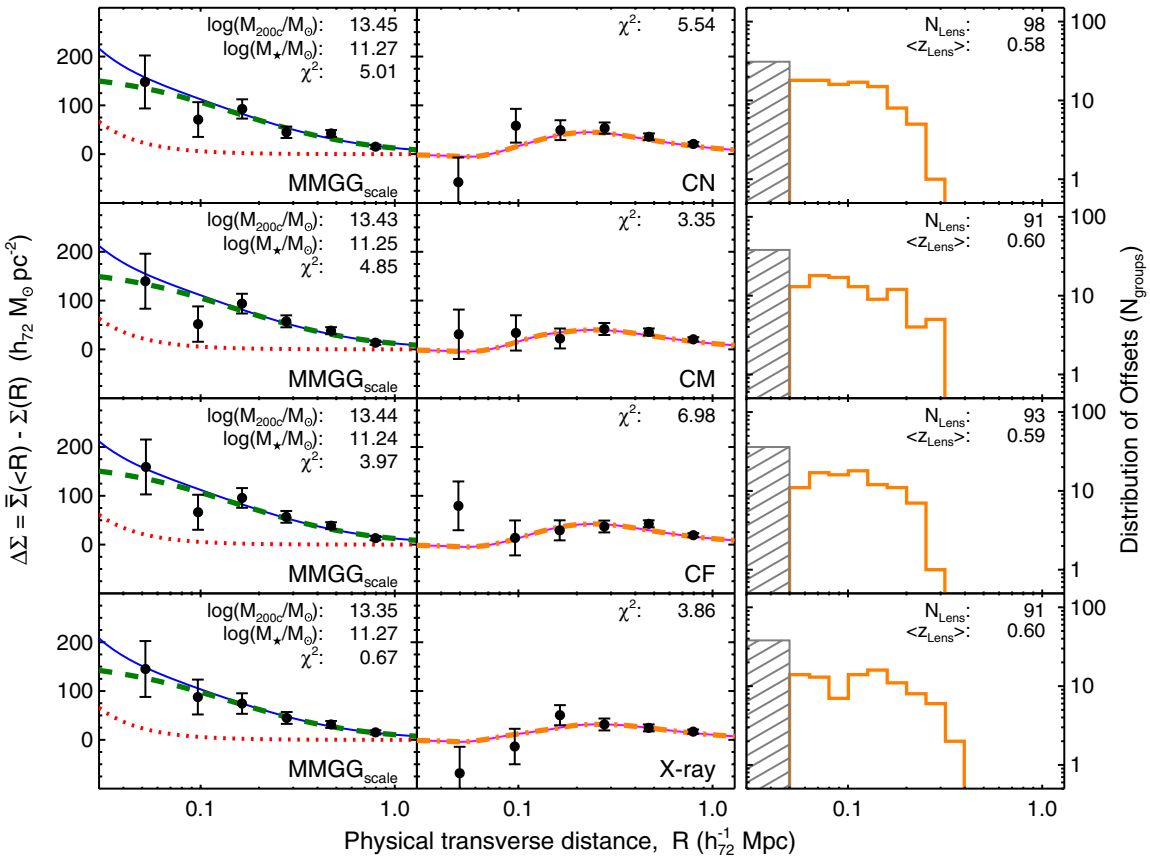

Figure 4. Lensing signal for subsets of groups where *centroid candidates* are offset from $MMGG_{scale}$ by >50 kpc. The left column shows the signal stacked around $MMGG_{scale}$, the middle column shows the signal stacked around an alternate candidate, and the right column shows the projected distribution of offsets between the two candidate positions. Models are discussed in the text, with line styles and colors as in Figure 3 and fit parameters stated within the left column. The number of groups with large offsets used in each row is stated in the right column, and the gray hashed boxes indicate the number of groups excluded from this analysis because the two candidates agree to within 50 kpc.

(A color version of this figure is available in the online journal.)

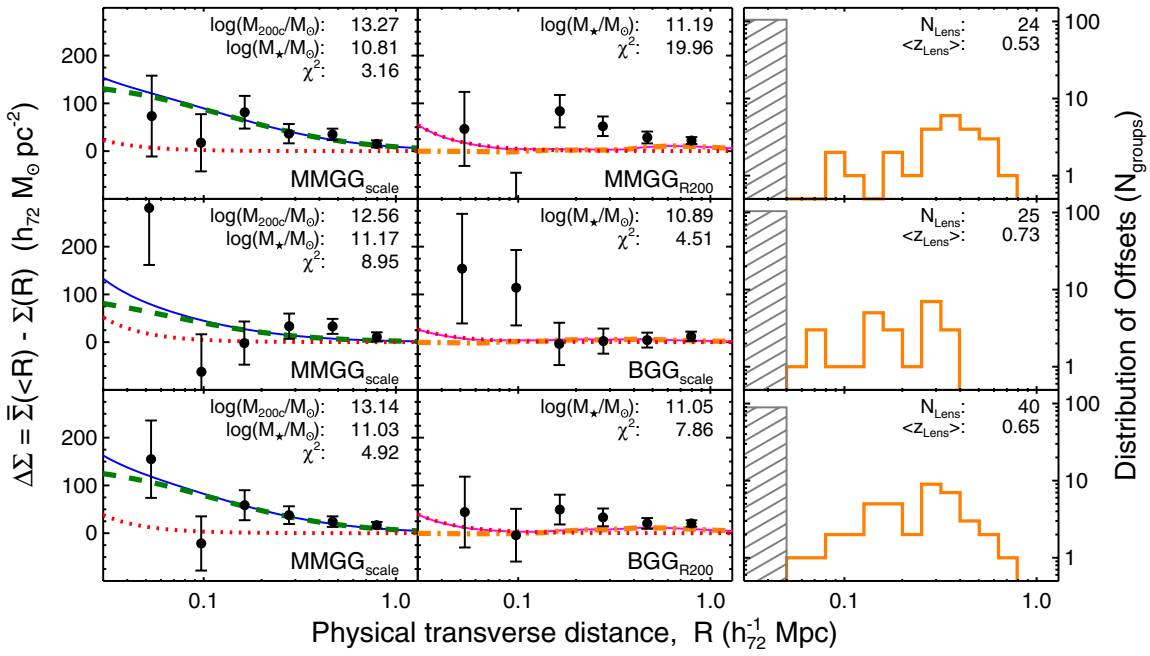

Figure 5. Lensing signal for subsets of groups where *galaxy candidates* are offset from $MMGG_{scale}$ by >50 kpc. Plot columns and style are the same as in Figure 4.

(A color version of this figure is available in the online journal.)

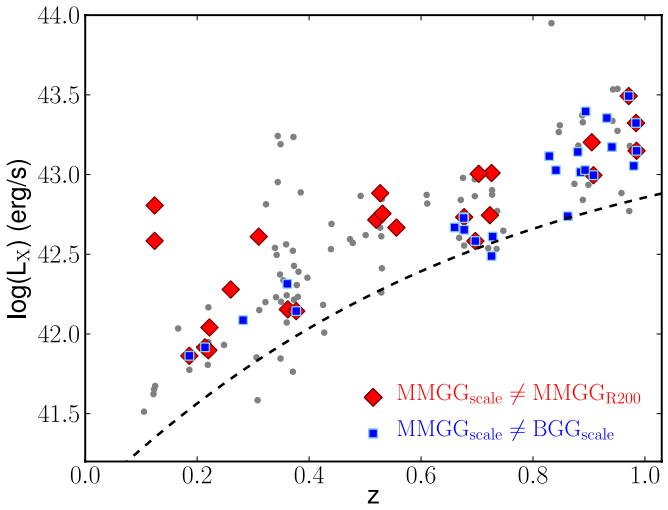

Figure 6. Distribution of redshifts and X-ray luminosities for the group sample. Cases where different galaxy candidates disagree are identified according to the legend. The dashed curve shows the 4σ X-ray flux limit of 1.0×10^{-15} erg cm^{-2} s^{-1} reached in 96% of the field converted to a limiting luminosity.

(A color version of this figure is available in the online journal.)

model. Though it appears that the BGG_{scale} produces a higher lensing signal than the $MMGG_{scale}$ at small radii in this direct comparison, that profile is not well fit by a centered NFW model, and the fitted mass is similarly low.

Figure 6 shows how two samples of groups with differing galaxy candidates are distributed in redshift and X-ray luminosity relative to the full sample of groups. Cases where the most massive group member lies in the outskirts ($MMGG_{scale} \neq MMGG_{R200}$) appear to be evenly distributed throughout the sample. Groups where the brightest galaxy near the X-ray position is not the most massive ($MMGG_{scale} \neq BGG_{scale}$) tend to be at higher redshifts, which can also be seen in the mean redshifts for the samples in Figure 5. This illustrates how an observed-frame selection of BCGs, like that used for BGG_{scale} here, tends to pick up bluer star-forming galaxies at higher redshifts.

The low masses shown in Figure 5 could be attributed to statistical fluctuations with the small sample size (24–40 groups, as compared with 91–98 groups in Figure 4). To test this idea, we performed jackknife tests using randomly selected samples of the same number of groups without replacement. In each of 1000 random samples we measured the lensing signal around $MMGG_{scale}$ and fit a model with a central point mass equal to the average stellar mass and a centered NFW with halo mass as a free parameter and concentration fixed. Of the 1000 random samples of 24 groups, 19% had a best-fit halo mass lower than that found for the sample of 24 groups where $MMGG_{scale} \neq MMGG_{R200}$. In samples of 25 groups, none had a lower best-fit halo mass than $\log(M_{200c}/M_{\odot}) = 12.57$, the value found for the sample with $MMGG_{scale} \neq BGG_{scale}$. And in samples of 40 groups, only 1% had a best-fit mass lower than the sample where $MMGG_{scale} \neq BGG_{R200}$. For a given X-ray luminosity, groups with discrepant galaxy candidate centers appear to have lower masses than the rest of the sample and in some cases more disturbed mass profiles.

Figure 6 shows a redshift dependence in the fraction of groups where the brightest galaxy (measured from the observer-frame F814W flux) does not have the highest stellar mass. High-redshift groups may have more disturbed lensing profiles for different reasons than having ambiguous galaxy center candidates, so we have repeated the jackknife tests restricting to groups at $z > 0.7$. Even among high-redshift systems, the groups with a brighter galaxy than $MMGG_{scale}$ are outliers; less than 1% of random samples of groups produce a best-fit mass lower than the samples where $MMGG_{scale} \neq BGG_{scale}$ or $MMGG_{scale} \neq BGG_{R200}$, while just 17% of random samples are fit by lower masses than the groups with $MMGG_{scale} \neq MMGG_{R200}$.

Visual inspections of the groups with discrepant galaxy candidates have not revealed obvious differences from the rest of the sample. Given the noisy lensing signal measured around such groups, one might worry that they are not real associations but chance projections. However, these groups are not preferentially found near the X-ray flux limit shown in Figure 6, and they do not have unusually low numbers of member galaxies associated with them, so they are unlikely to be impurities in the group sample.

Groups with multiple massive galaxies and disturbed density profiles are likely to have merged recently, a point we discuss further in Section 6.

5.3. Model Uncertainties

Having established that the lensing data can be used to constrain the choice of a tracer for the centers of mass of halos, we would like to know how well a given candidate actually traces halo centers. In this section we explore a more general model to see how certain assumptions, namely, the mass–concentration relation and the form of the central mass component, affect our results.

The results shown in the previous section suggest that galaxy candidates trace the halo centers better than centroid candidates, because the stacked lensing signal on small scales is greater when centered on a galaxy. While the model used to fit the signal for galaxy candidates includes a component to account for the stellar mass that exists in galaxy candidates but not in centroid candidates, it is plausible that we have underestimated the amount of mass in the central galaxies, either in stars and baryons or in a dark matter subhalo. In a typical halo model the central galaxy has no subhalo, so in the latter scenario the galaxy candidate could actually be a satellite or the system may be unrelaxed. Detailed modeling of strong and weak lensing observations of individual clusters has found evidence for subhalos around member galaxies even near cluster centers (Natarajan et al. 2007, 2009). Additional mass in the central term $\Sigma_{gal}(R)$ could hide significant offsets between the galaxy candidates and host halos, effectively filling in the decrement at small radii in the halo term $\Sigma_{halo}(R)$.

To address this degeneracy, we apply our full model with an additional mass component around the galaxy candidate, in addition to the point source representing the stellar mass. We use the functional form of a truncated non-singular isothermal sphere (Pastor Mira et al. 2011)

$$\rho(r) = \frac{\rho_0}{\left(1 + r^2/r_{core}^2\right)\left(1 + r^2/r_{cut}^2\right)}. \quad (13)$$

We fix the core radius $r_{core} = 0.1$ kpc and set the truncation radius r_{cut} to the distance at which the local mass densities of the subhalo and halo components are equal, as measured along the line connecting their centers assuming an offset distance σ_{off}. To facilitate comparisons with the stellar mass, we cast the normalization of the model in terms of a free parameter M_{sub} (instead of ρ_0), which we will refer to as the subhalo mass,

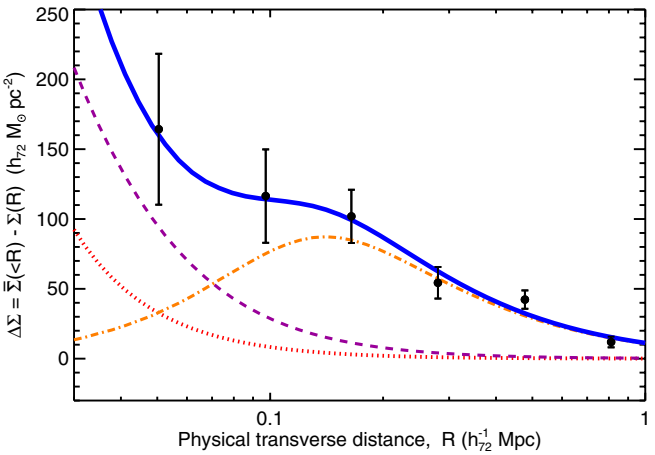

Figure 7. Stacked lensing signal for 85 groups where galaxy candidates agree. Model curves show the maximum likelihood solution for an offset NFW halo (orange dot-dashed), subhalo (purple dashed), and a point source for the stellar mass (red dotted), along with the sum (thick solid blue). There are degeneracies among some fit parameters; for example, a model with smaller centering offsets and a less massive subhalo also fits the data.

(A color version of this figure is available in the online journal.)

defined as the mass enclosed within 5 kpc, the mean half-light radius for our sample. Since the core radius is much smaller than our innermost lensing measurement, the exact value chosen does not influence our results. The choice of truncation radius and functional form of the subhalo mass profile does affect the mass normalization, but the qualitative shapes of the parameter degeneracies are consistent for a variety of truncation schemes and for mass profiles that are isothermal, or nearly so, across the inner few tens of kpc. However, if the subhalo component is not truncated at all, or if it is modeled instead as an NFW profile as Pastor Mira et al. find in simulations with subhalos, its mass can become degenerate with the full halo mass.

For a given lensing signal, a larger halo concentration can also compensate for some miscentering effects, so we free the c_{200c} parameter to study the degeneracy with σ_{off} without the restrictions of the model for concentration used before. In practice, concentration is not well constrained by this data set, so a prior is still needed to restrict the range of values when fitting.

An additional model uncertainty comes from the form of the distribution of offsets $P(R_{off})$ that is used. The offsets between galaxy candidates in Figure 1 appear to support the models used by Johnston et al. (2007b) and Oguri et al. (2010), with a significant fraction of agreement between candidates along with a wide tail in the distribution. To avoid the need for additional free parameters describing both well-centered and miscentered populations in the offset distribution, we attempt to select a clean sample of groups and constrain the scale of offsets between the candidate galaxy center and the halo center assuming the single distribution given in Equation (9). We test this model on the sample of groups for which the four galaxy candidates agree, i.e., where the brightest and most massive group members are one and the same, and where this galaxy lies within an NFW scale radius of the X-ray centroid. There are 85 groups with such unambiguous galaxy centers.

The lensing signal for these groups stacked around the galaxy candidate is shown in Figure 7. To summarize our model, we fit the signal with an NFW halo and a truncated isothermal subhalo of the form in Equation (13) in addition to a point mass fixed by the photometric stellar mass. The point mass is fixed at the center of the subhalo, which is allowed to be offset from the center of the halo. This leaves four free parameters: the halo mass M_{200c} and concentration c_{200c}, the offset scale σ_{off} between the galaxy and halo, and the subhalo mass normalization M_{sub}.

Figure 8 shows the results of the MCMC analysis exploring this parameter space. Each panel with blue contours shows the 68% and 95% regions of the joint posterior probabilities for a pair of parameters, marginalizing over the other parameters. The top panel in each column shows for each parameter the arbitrarily normalized prior from Table 1 (dashed green curves) and the one-dimensional posterior probabilities (black histograms) while marginalizing over the other parameters. Note that the data are unable to constrain a lower limit on the subhalo mass or an upper limit to the concentration, so the posterior distributions are sensitive to our priors in those regions.

The data are consistent with a model in which there are no subhalos around the candidate central galaxies, though a value comparable to the average stellar mass of the galaxies is preferred, and significantly more massive subhalos are ruled out. We emphasize that the stellar mass is already included in the model as a point source, so the subhalo component represents mass in excess of the stellar mass that was estimated from the photometry. Recall that the M_{sub} is defined as the subhalo mass within the typical half-light radius of 5 kpc; integration of Equation (13) out to large radii for the maximum likelihood parameters gives a *total* subhalo mass of roughly five times the observed stellar mass component. The truncation radius for this model is 21 kpc. The preference for a nonzero subhalo mass may simply indicate that the photometric stellar mass is underestimated,[12] or that the point source model for the stellar term is insufficient. A subset of correctly centered groups (or an excess at small scales in the offset distribution relative to the model) could also explain the signal that we have fitted as a subhalo component. The halo mass is well constrained and consistent with the values measured for the full group sample with the simpler model in Section 5.1. The data prefer a higher value of c_{200c} than the Zhao et al. (2009) prediction for this halo mass and redshift, but the concentration is not well constrained. For the offset distribution, the data are consistent with no offsets between the central galaxy candidates and the halo centers, though a value of roughly 50 kpc is preferred. Large offsets ($\sigma \gtrsim 100$ kpc) are ruled out for an offset model of a single two-dimensional Gaussian distribution, though individual outliers may exist. On average, massive galaxies trace halo centers quite well.

There are degeneracies between the offset distance scale and the subhalo mass as well as the halo concentration. If the subhalo mass within 5 kpc is smaller than $\sim 10^{11}\ M_{\odot}$, the offset scale must be smaller than 50 kpc, but for larger subhalo masses the offset scale can reach 100 kpc. A constraint on the total mass enclosed within small scales, perhaps from strong lensing or measurements of stellar velocity dispersions for the central galaxies, could improve constraints on σ_{off}. Similarly, c_{200c} and σ_{off} are correlated, with higher concentrations corresponding to larger offsets. Thus, when modeling a given lensing signal, if miscentering is not taken into account, it can lead to an underestimate of the concentration.

[12] Stellar masses used in this work have been derived assuming a Chabrier (2003) initial mass function (IMF). Recent suggestions of a steeper subsolar IMF for early-type galaxies could explain this discrepancy (e.g., Auger et al. 2010; van Dokkum & Conroy 2010).

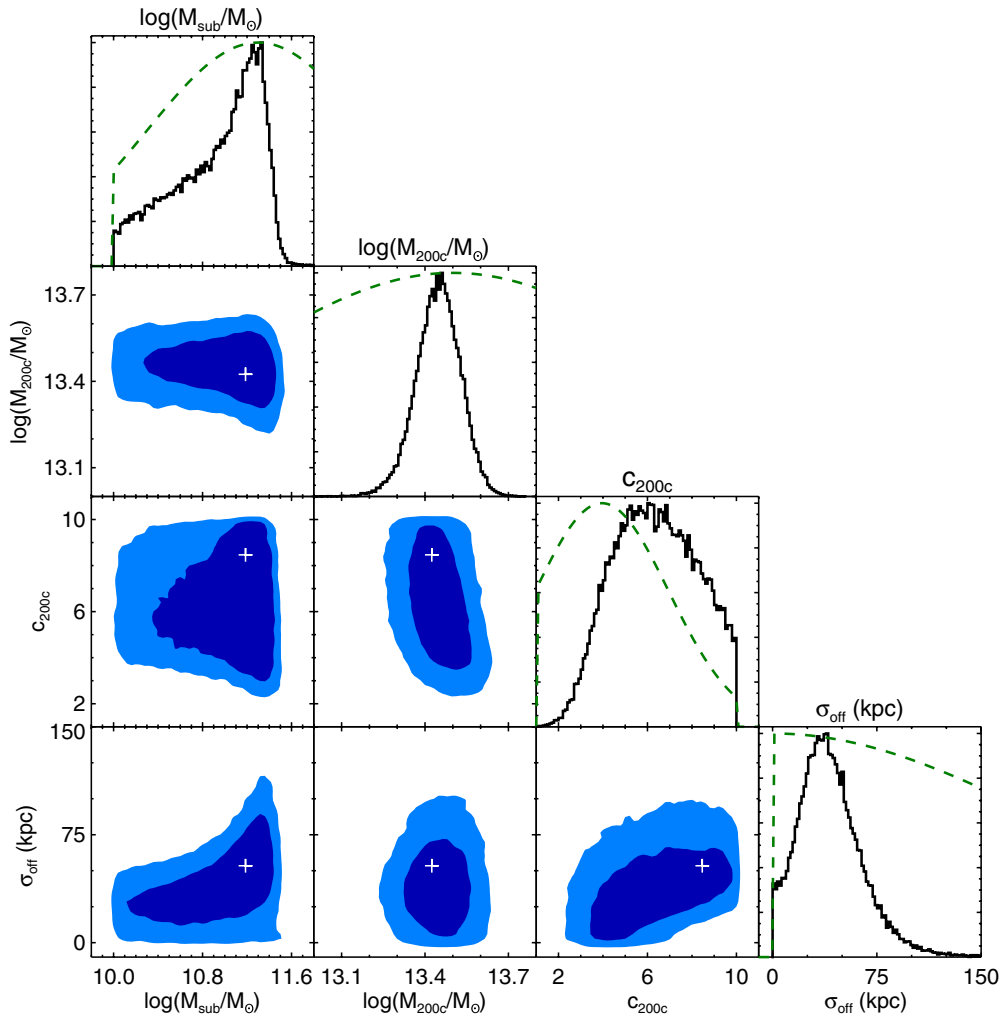

Figure 8. Posteriors for the four parameters of a general offset model discussed in the text, applied to the lensing signal from Figure 7. Blue contours show 68% and 95% regions for the pair of parameters noted along the axes, marginalized over the other parameters. White crosses mark the maximum likelihood parameters. Top panels show the posterior distributions for single parameters while marginalizing over the others (black histograms), along with arbitrarily normalized priors (green dashed curves).

(A color version of this figure is available in the online journal.)

6. DISCUSSION

Finding the centers of mass for dark matter halos presents both an observational challenge and an opportunity to study the interplay between halos and central galaxies. In this paper, we have presented a method to test different tracers of group and cluster centers by comparing the weak lensing signal stacked around their positions. Our approach can in principle be applied to any analysis that would be affected by miscentering. For instance, centering algorithms can also be tested using satellite kinematics by identifying the candidate that is nearest to the dynamical center when averaging over the ensemble. The spatial clustering of galaxies can also provide centering information; in practice, the peaks in the galaxy density field are generally used in defining optical cluster catalogs, but clustering data could also be used to optimize the determination of their centers. Additionally, these approaches to optimizing the centers of a halo catalog can be fed back into algorithms used to find halos and their centers, allowing a more probabilistic approach to deal with cases where centering is uncertain.

With X-ray-detected galaxy groups in the COSMOS field, we find that individual bright and massive galaxies trace the centers of halos better than the nominal X-ray centroid or the mean position of group members, even when weighted by luminosity or stellar mass. Offsets between the X-ray centroids and candidate central galaxies are primarily due to the large uncertainties in the X-ray positions, which can reach roughly 200 kpc. Centroids based on the mean positions of galaxies also have significant uncertainties, though some offsets exceed the estimated errors. More stringent constraints on intrinsic offsets between centroid candidates and halo centers could be obtained with deeper, high-resolution X-ray or SZ data, or with a sample of massive clusters and more member galaxies.

For each pair of galaxy candidates defined in Section 3, roughly 20%–30% of groups have ambiguous centers. Either the most massive galaxy lies far from the X-ray position, or the brightest galaxy is not the most massive. Only two-thirds (85 out of 129) of the groups show complete agreement between all four galaxy candidates, which underlines the importance of testing any choice of center in a group or cluster catalog.

The results of Figure 5 and the jackknife tests described in Section 5.2 suggest that groups with ambiguous galaxy centers have low masses for their X-ray luminosities or disturbed halo mass profiles. A connection between centering offsets and

the dynamical state of halos has been seen in observational studies (e.g., Forman & Jones 1982; Katayama et al. 2003; Sanderson et al. 2009) and simulations (e.g., Cohn & White 2005; Poole et al. 2006; Macciò et al. 2007; Neto et al. 2007; Skibba & Macciò 2011). The ability to identify unusual or unrelaxed groups and clusters with a simple observable such as having different candidate centers could prove useful when trying to select a clean sample of relaxed systems. Further studies connecting lensing measurements with member galaxy properties such as the distribution of colors may provide a clearer picture of the impact of halo mergers on galaxies and star formation. Similarly, a more general analysis of the gaps in stellar mass or luminosity and the spatial separation between massive member galaxies would complement the restricted set of center candidates studied here.

There are several reasons why candidate centers can be offset from halo centers. Interlopers or incompleteness in the group member sample can result in the wrong galaxies being selected. Satellite galaxies can be more massive or luminous than centrals due to scatter in the relation linking the observable property to the mass of a halo or subhalo. In Paper I, we presented tests of our group membership and centering algorithm on mock catalogs designed to reflect the real uncertainties in X-ray positions and photometric redshifts. In that analysis, 77% of central galaxies were correctly identified as the $\mathrm{MMGG_{scale}}$. The most common failure mode was the selection of satellites as $\mathrm{MMGG_{scale}}$ because they had higher stellar masses than the true centrals, which happened in 12% of cases. The frequency of this occurrence depends on the way we populate halos with mock galaxies following the stellar-mass–halo-mass relation of Leauthaud et al. (2012), but we note that scatter in this relation is consistent with that found in other analyses (Yang et al. 2009; More et al. 2009; Reddick et al. 2012). The remaining centering failures were evenly split between cases where X-ray errors misplaced the search region and photometric redshift errors scattered centrals out of their groups.

Observational uncertainties, such as scatter in stellar mass estimates ($\sim$0.2 dex) and catastrophic errors in photometric redshifts (for $\lesssim$ a few percent of objects in our COSMOS sample), add to this scatter and increase the chances that a satellite is incorrectly identified as the central galaxy. Furthermore, merging activity is not modeled in the mock catalogs, so these effects together can account for the $\sim$30% of observed groups where galaxy candidates disagree. The offsets seen between centroid candidates (CN, CM, CF, and X-ray) are consistent with being due primarily to the large observational uncertainties in their positions.

The offsets measured in this paper are significantly smaller than the distribution measured from mock catalogs by Johnston et al. (2007b). This could be due in part to our choice of offset model; in Sections 5.1 and 5.3 we assumed a single Rayleigh distribution of offsets, whereas Johnston et al. separated groups that were correctly centered from those that were miscentered. Our aim in Section 5.1 was simply to estimate a typical offset scale for comparing candidate centers, and in Section 5.3 we selected a sample where centering seemed unambiguous to study up close the offsets of massive galaxies that could be sloshing around halo centers. The offsets found in Section 5.3 are comparable to the smaller component of the offset distribution measured by Oguri et al. (2010). While they are fairly small, modeling degeneracies with the subhalo mass and halo concentration increase their uncertainty. Future analyses of halo properties may benefit from including a range of models for the distribution of offsets, if the data can constrain a larger number of parameters.

Another important difference between our analysis and that of Johnston et al. is that the maxBCG clusters are detected as optical galaxy overdensities, whereas the COSMOS groups studied here are detected in X-ray emission, which traces the dense regions near the centers of halos, offering a better starting point for finding the centers of halos. When comparing the effects of miscentering for different cluster catalogs, it is also worth noting that more massive clusters are larger, so offsets of a given distance can be more easily detected than in less massive systems.

Further investigations with simulations could improve our understanding of some issues with centering (e.g., Macciò et al. 2007; Neto et al. 2007; Hilbert & White 2010; Behroozi et al. 2011; Dietrich et al. 2012; Power et al. 2012). There is a similar ambiguity when defining the center of a simulated dark matter halo, since there can be offsets between the position of the most bound particle, the mass density peak, and the centroid of mass with a given smoothing scale. Offsets between these positions in simulations have been shown to correlate with the dynamical state of a halo, with larger offsets seen in less relaxed halos that have experienced a recent merger. Projecting the matter density in simulated halos to compare with the observed lensing signals could help explain the poor fits to NFW profiles and unusually low masses we obtain from samples with ambiguous centers. Similarly, a better understanding of the form and evolution of halo and subhalo mass profiles, due to effects like gas cooling or heating and tidal stripping, could improve our modeling.

Finally, we consider the implications of miscentering for cosmological analyses. The abundance of massive halos is sensitive to the amplitude of matter fluctuations and the growth history of the universe, and the precise determination of group and cluster masses is a critical aspect of this probe. Mandelbaum et al. (2010) have studied the effects of miscentering on mass estimates for massive halos using simulated data and analytical profiles, assuming the distribution of offsets from the mock catalogs of Johnston et al. (2007b). For clusters at the upper end of our mass range ($\sim 10^{14}\,M_{\odot}$), they find that the weak lensing mass is underestimated by 25%–30% if miscentering is ignored, and that this effect is stronger for less massive halos (see their Figure 3). They also show that the accuracy of mass estimates depends on the assumed concentration, as well as the inner and outer radius measured, and suggest excising the inner regions from the analysis because of these uncertainties. In a separate study, Mandelbaum et al. (2008) measured the mass–concentration relation for several samples of galaxies and clusters, including the maxBCG sample. Miscentering of clusters is also a concern for measuring concentrations, producing values that are biased low if the effect is ignored. Mandelbaum et al. (2008) argued that the miscentering distribution from Johnston et al. (2007b) may be overestimated, based on the concentrations they derived from lensing and by comparison with the distribution of offsets between BCGs and X-ray peaks in a subsample of clusters (Koester et al. 2007a). Still, they had to trade off statistical power by excluding data at small radii to reduce systematic uncertainties from modeling the distribution of offsets.

In this paper, we have endeavored to improve the accuracy of finding halo centers and to provide constraints on the distribution of offsets between observational tracers and underlying mass centers. With more accurate centers (and uncertainties on those positions), we can more reliably use data at small radii and

improve statistical constraints from group and cluster surveys. Table 2 suggests that the halo mass inferred from the lensing signal stacked around our galaxy candidates is affected at the 5%–10% level if miscentering is ignored. This is significantly smaller than the bias seen by Mandelbaum et al. (2010) despite the trend that masses are increasingly underestimated for lower mass halos. We attribute the difference to the smaller offsets seen in this sample compared to the miscentering distribution used by Johnston et al. (2007b), where a fraction of groups had a distribution of offsets with $\sigma_{\rm off} = 420h^{-1}$ kpc. However, we also use a different model for the offset distribution and can see in Table 2 that the masses estimated from centroid candidates are more biased (15%–30%) when miscentering is not addressed in the model. The statistical uncertainties on our halo mass estimates are still comparable to the centering bias, and with this sample we are currently unable to put a significant constraint on the halo concentration. But with larger group and cluster samples, our approaches to optimizing the choice of halo centers and modeling the distribution of offsets will enable better constraints on halo mass profiles for both astrophysical and cosmological applications.

7. SUMMARY AND CONCLUSIONS

We summarize the main results of this paper as follows:

1. In our data set, different definitions of group centers do not always agree and occasionally show large offsets from one another. Candidate centers based on the locations of the brightest or most massive galaxy differ in 20%–30% of cases with a wide range of offsets. Centroids based on the mean position of member galaxies or X-ray flux have offsets from other center definitions that are roughly consistent with their larger statistical uncertainties ($\sim$50–150 kpc).
2. The offsets between centers produce a measurable signal in the lensing profile. Stacking the signal around a bright or massive galaxy tends to produce a larger signal at small scales than any centroid not located on a galaxy, and the difference in these signals is greater than expected from the stellar mass of the galaxy.
3. Among the candidate centers we have tested, the brightest or the most massive galaxies near the X-ray centroid appear to be the best tracers of the center of mass of halos. Centering definitions based on the centroid of member galaxies have larger offsets and uncertainties.
4. Groups that have ambiguous centers because of multiple bright or massive galaxies have lensing signals that suggest a lower mass than expected given their X-ray luminosity and in some cases appear disturbed. These are possibly merging systems, and the property of having discrepant candidate centers gives a simple observational indicator to identify them.
5. In groups with a clear central galaxy, offsets between the galaxy and the halo center are fairly small ($\lesssim$75 kpc). The offset is somewhat degenerate with the amount of substructure around the galaxy and with the concentration of the group halo.

These findings apply to our group sample, but our approach can readily be applied to other group and cluster data sets and to different analyses such as satellite dynamics and richness-based mass estimators. Given the level of disagreement among our candidate centers, we advise testing different centers to determine the degree to which centering choices affect a given analysis. Our finding that groups with ambiguous centers are less massive for their X-ray luminosity or have disturbed mass profiles suggests that these groups could be identified and excluded if an analysis calls for a clean sample of halos. Additionally, a probabilistic approach to centering algorithms could provide information about the confidence in a given center allowing for appropriate weighting of different systems.

Much larger samples of groups and clusters are being constructed with ongoing and upcoming surveys, such as the South Pole Telescope, Atacama Cosmology Telescope, the Dark Energy Survey, and eROSITA. This initial study with a modestly sized sample of groups benefits from high-resolution X-ray selection, which provides a good starting point for finding centers, but a similar approach can be applied to optical or SZ-selected catalogs. With larger samples, we can hope to improve constraints on the density profiles of dark matter halos, including their concentration and inner slope, as well as the mass distribution in subhalos and the effects of mergers. Additional constraints on the mass distribution from strong lensing or stellar kinematics can provide interesting constraints on a range of scales and improve models for the distribution of offsets between galaxies and halo centers.

We thank Uros Seljak and Priya Natarajan for constructive comments on a draft of the paper, as well as Ami Choi and David Schlegel for helpful discussions. M.R.G. has been supported by the US Department of Energy's Office of High Energy Physics (DE-AC02-05CH11231) and a Graduate Research Fellowship from the US National Science Foundation. This work was also supported by World Premier International Research Center Initiative (WPI Initiative), MEXT, Japan.

We gratefully acknowledge the contributions of the entire COSMOS collaboration, consisting of more than 70 scientists. More information on the COSMOS survey is available at http://www.astro.caltech.edu/cosmos. This research has made use of the NASA/IPAC Infrared Science Archive, which is operated by the Jet Propulsion Laboratory, California Institute of Technology, under contract with the National Aeronautics and Space Administration.

REFERENCES

Auger, M. W., Treu, T., Gavazzi, R., et al. 2010, ApJ, 721, L163
Behroozi, P. S., Wechsler, R. H., & Wu, H.-Y. 2011, arXiv:1110.4372
Berlind, A. A., Frieman, J., Weinberg, D. H., et al. 2006, ApJS, 167, 1
Bradač, M., Allen, S. W., Treu, T., et al. 2008, ApJ, 687, 959
Capak, P., Aussel, H., Ajiki, M., et al. 2007, ApJS, 172, 99
Carlberg, R. G., Yee, H. K. C., Morris, S. L., et al. 2001, ApJ, 552, 427
Chabrier, G. 2003, PASP, 115, 763
Clowe, D., Bradač, M., Gonzalez, A. H., et al. 2006, ApJ, 648, L109
Clowe, D., Gonzalez, A., & Markevitch, M. 2004, ApJ, 604, 596
Cohn, J. D., & White, M. 2005, Astropart. Phys., 24, 316
Cooray, A., & Sheth, R. 2002, Phys. Rep., 372, 1
Dietrich, J. P., Böhnert, A., Lombardi, M., Hilbert, S., & Hartlap, J. 2012, MNRAS, 419, 3547
Dunkley, J., Komatsu, E., Nolta, M. R., et al. 2009, ApJS, 180, 306
Elvis, M., Civano, F., Vignali, C., et al. 2009, ApJS, 184, 158
Finoguenov, A., Connelly, J. L., Parker, L. C., et al. 2009, ApJ, 704, 564
Finoguenov, A., Watson, M. G., Tanaka, M., et al. 2010, MNRAS, 403, 2063
Forman, W., & Jones, C. 1982, ARA&A, 20, 547
George, M. R., Leauthaud, A., Bundy, K., et al. 2011, ApJ, 742, 125
Gladders, M. D., & Yee, H. K. C. 2000, AJ, 120, 2148
Guzik, J., & Seljak, U. 2002, MNRAS, 335, 311
Hao, J., McKay, T. A., Koester, B. P., et al. 2010, ApJS, 191, 254
Hasinger, G., Cappelluti, N., Brunner, H., et al. 2007, ApJS, 172, 29
Hikage, C., Takada, M., & Spergel, D. N. 2012, MNRAS, 419, 3457
Hilbert, S., & White, S. D. M. 2010, MNRAS, 404, 486
Hudson, M. J., Gwyn, S. D. J., Dahle, H., & Kaiser, N. 1998, ApJ, 503, 531
Ilbert, O., Capak, P., Salvato, M., et al. 2009, ApJ, 690, 1236

Jee, M. J., Dawson, K. S., Hoekstra, H., et al. 2011, ApJ, 737, 59
Johnston, D. E., Sheldon, E. S., Tasitsiomi, A., et al. 2007a, ApJ, 656, 27
Johnston, D. E., Sheldon, E. S., Wechsler, R. H., et al. 2007b, arXiv:0709.1159
Katayama, H., Hayashida, K., Takahara, F., & Fujita, Y. 2003, ApJ, 585, 687
Koekemoer, A. M., Aussel, H., Calzetti, D., et al. 2007, ApJS, 172, 196
Koester, B. P., McKay, T. A., Annis, J., et al. 2007a, ApJ, 660, 239
Koester, B. P., McKay, T. A., Annis, J., et al. 2007b, ApJ, 660, 221
Leauthaud, A., Finoguenov, A., Kneib, J.-P., et al. 2010, ApJ, 709, 97
Leauthaud, A., Massey, R., Kneib, J.-P., et al. 2007, ApJS, 172, 219
Leauthaud, A., Tinker, J., Bundy, K., et al. 2012, ApJ, 744, 159
Lilly, S. J., Le Brun, V., Maier, C., et al. 2009, ApJS, 184, 218
Lin, Y.-T., & Mohr, J. J. 2004, ApJ, 617, 879
Macciò, A. V., Dutton, A. A., van den Bosch, F. C., et al. 2007, MNRAS, 378, 55
Mandelbaum, R., Seljak, U., Baldauf, T., & Smith, R. E. 2010, MNRAS, 405, 2078
Mandelbaum, R., Seljak, U., Cool, R. J., et al. 2006a, MNRAS, 372, 758
Mandelbaum, R., Seljak, U., & Hirata, C. M. 2008, J. Cosmol. Astropart. Phys., JCAP08(2008)006
Mandelbaum, R., Seljak, U., Kauffmann, G., Hirata, C. M., & Brinkmann, J. 2006b, MNRAS, 368, 715
Massey, R., Kitching, T., & Nagai, D. 2011, MNRAS, 413, 1709
Massey, R., Stoughton, C., Leauthaud, A., et al. 2010, MNRAS, 401, 371
Miralda-Escude, J. 1991, ApJ, 370, 1
More, S., van den Bosch, F. C., Cacciato, M., et al. 2009, MNRAS, 392, 801
Natarajan, P., De Lucia, G., & Springel, V. 2007, MNRAS, 376, 180
Natarajan, P., & Kneib, J.-P. 1997, MNRAS, 287, 833
Natarajan, P., Kneib, J.-P., Smail, I., et al. 2009, ApJ, 693, 970
Navarro, J. F., Frenk, C. S., & White, S. D. M. 1996, ApJ, 462, 563
Neto, A. F., Gao, L., Bett, P., et al. 2007, MNRAS, 381, 1450
Oguri, M., Takada, M., Okabe, N., & Smith, G. P. 2010, MNRAS, 405, 2215
Pastor Mira, E., Hilbert, S., Hartlap, J., & Schneider, P. 2011, A&A, 531, A169
Poole, G. B., Fardal, M. A., Babul, A., et al. 2006, MNRAS, 373, 881
Power, C., Knebe, A., & Knollmann, S. R. 2012, MNRAS, 419, 1576
Reddick, R. M., Wechsler, R. H., Tinker, J. L., & Behroozi, P. S. 2012, arXiv:1207.2160
Rhodes, J., Refregier, A., & Groth, E. J. 2000, ApJ, 536, 79
Rhodes, J. D., Massey, R. J., Albert, J., et al. 2007, ApJS, 172, 203
Robotham, A. S. G., Norberg, P., Driver, S. P., et al. 2011, MNRAS, 416, 2640
Rozo, E., Rykoff, E., Koester, B., et al. 2011, ApJ, 740, 53
Sanderson, A. J. R., Edge, A. C., & Smith, G. P. 2009, MNRAS, 398, 1698
Scoville, N., Aussel, H., Brusa, M., et al. 2007, ApJS, 172, 1
Shan, H., Qin, B., Fort, B., et al. 2010, MNRAS, 406, 1134
Sheldon, E. S., Annis, J., Böhringer, H., et al. 2001, ApJ, 554, 881
Skibba, R. A., & Macciò, A. V. 2011, MNRAS, 416, 2388
Skibba, R. A., van den Bosch, F. C., Yang, X., et al. 2011, MNRAS, 410, 417
Smith, G. P., Kneib, J.-P., Smail, I., et al. 2005, MNRAS, 359, 417
Sunyaev, R. A., & Zeldovich, Y. B. 1972, Comments Astrophys. Space Phys., 4, 173
van Dokkum, P. G., & Conroy, C. 2010, Nature, 468, 940
White, R. A., Bliton, M., Bhavsar, S. P., et al. 1999, AJ, 118, 2014
Wojtak, R., Hansen, S. H., & Hjorth, J. 2011, Nature, 477, 567
Wright, C. O., & Brainerd, T. G. 2000, ApJ, 534, 34
Yang, X., Mo, H. J., & van den Bosch, F. C. 2009, ApJ, 695, 900
Yang, X., Mo, H. J., van den Bosch, F. C., et al. 2006, MNRAS, 373, 1159
Yang, X. H., Mo, H. J., Kauffmann, G., & Chu, Y. Q. 2003, MNRAS, 339, 387
Zehavi, I., Zheng, Z., Weinberg, D. H., et al. 2005, ApJ, 630, 1
Zhao, D. H., Jing, Y. P., Mo, H. J., & Börner, G. 2009, ApJ, 707, 354